Conf-9206201--4

UCRL-JC-110753
PREPRINT

Applications of Energy Loss Contrast STIM

G. Bench
A. Saint
G.J.F. Legge
M. Cholewa

This paper was prepared for submittal to the
3rd International Conference on Nuclear
Microprobe Technology and Applications
Uppsala, Sweden
June 8-12, 1992

May 26, 1992

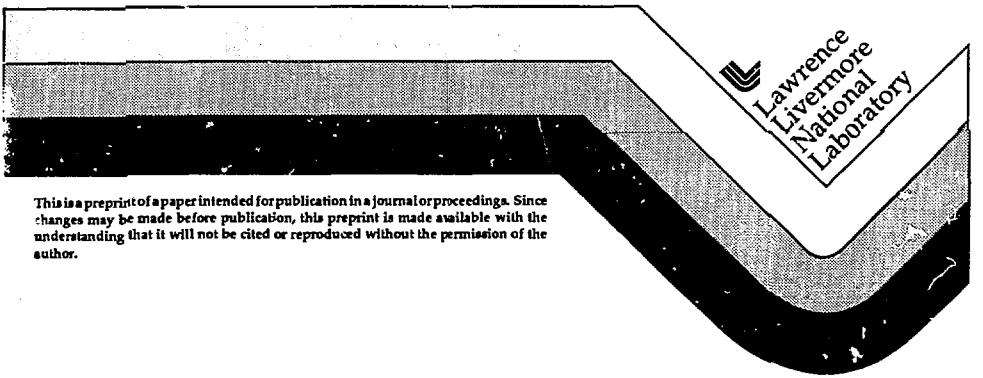

UCRL-JC—110753

DE92 017254

Applications of Energy Loss Contrast STIM.

G.Bench[1], A. Saint, G.J.F. Legge and M. Cholewa.

Micro Analytical Research Centre, School of Physics, University of Melbourne, Parkville, Victoria, 3052, Australia.

[1] Present Address: Center for Accelerator Mass Spectrometry, Lawrence Livermore National Laboratory, Physics Department, P.O. Box 808, L-397, Livermore, CA 94550, U.S.A.

Abstract.

Scanning Transmission Ion Microscopy (STIM) with energy loss contrast is a quantitative imaging technique. A focussed MeV ion microbeam is scanned over the sample and measured energy losses of residual ions at each beam location are used to provide the contrast in the image. The technique is highly efficient as almost every ion carries useful information from which quantitative data can be obtained. The high efficiency of data collection at present necessitates the use of small beam currents. Therefore small apertures can be used and fine spatial resolution can be achieved. High efficiency also makes it possible to collect large data sets for high definition imaging with a small radiation dose. Owing to the simple relationship between energy loss and areal density, STIM with energy loss contrast can provide a quantitative image that can be used to obtain areal density information on the sample. These areal density maps can be used not only to provide a high resolution image of the sample but also to normalise Particle Induced Xray Emission (PIXE) data. The small radiation dose required to form these

areal density maps also allows one to use STIM with energy loss contrast to quantitatively monitor ion beam induced specimen changes caused by higher doses and dose rates used in other microanalytical techniques. STIM with energy loss contrast also provides the possibility of stereo imaging and ion microtomography. STIM has also been used in conjunction with channeling to explore transmission channeling in thin crystals. This paper will discuss these applications of STIM with energy loss contrast and look at further developments from them.

Introduction.

The use of a scanned, focussed, MeV energy microbeam of accelerated ions for energy loss transmission imaging was originally investigated by Overley *et al.* [1] and Sealock *et al.* [2] in 1983 and Fischer [3] in 1985. With this Scanning Transmission Ion Microscopy (STIM) technique a focussed MeV ion microbeam is scanned over the sample and the residual energies of the transmitted ions are, at present, usually recorded by an energy dispersive solid state detector placed at 0^0 to the incident beam. Images are then formed from measured ion energy losses at each picture element or pixel. This technique provides a high resolution non-surface imaging mode for the MeV ion microprobe.

In the past decade STIM has developed from a simple imaging technique, to a versatile analytical technique with a wide range of applications. The use of STIM to complement PIXE analysis has been explored [4, 5]. STIM areal density maps have been used for mass normalisation of PIXE images [4, 5]. The same areal density maps can provide complementary information, often at finer spatial resolutions, that can help identify microstructure associated with element localisations [5]. Energy loss STIM in air has been used to image small living animals [6]. The use of stereo-STIM to provide information on the spatial distribution and orientation of small features within a specimen has been developed [5, 7]. The development of STIM Tomography (ion microtomography) enables one to characterise the density distribution within a specimen [8]. The development of channeling STIM provides a high spatial resolution ion channeling technique which causes minimal damage to the specimen and which is very sensitive to small variations

in crystal quality [9]. In this paper we will discuss the current state of these STIM techniques and indicate possible directions in which they may head.

Image formation for STIM with a MeV Ion Microprobe.

For STIM with MeV ion microprobes the incident ion species and energy are usually chosen so that the incident beam can pass through the sample and ion energy loss is primarily due to interactions with specimen electrons. Several STIM techniques with a MeV ion microprobe [1, 2, 3, 10, 11] have been reported where images are formed from measured ion energy losses at each incident beam location. Although images can be formed in principle from one ion per pixel [1], for higher definition images several particles are required to reduce noise and improve contrast. Typically images are formed from $\sim$ 5 to 20 ions per pixel.

To form an image, a number is derived from data accumulated at each beam position and the associated image pixel is intensified according to that number. For STIM, three of the more commonly used strategies are summing of ions within an energy window, energy averaging and median filtering.

Sealock *et al.* [2] and Fischer [3] examined the use of forming images by counting the number of ions within an energy window. This is the method of imaging commonly used in PIXE analysis, with window boundaries selected according to characteristic x-ray energy. With this option, counting statistics will produce noisy images unless the number of events per pixel is substantial. As only a few ions per pixel are generally collected with STIM and as, in many instances, one would like to accurately determine the energy loss at each pixel (there is only one true areal density at any pixel) windowing the collected data is often not a suitable technique, although it has been used, with some success, to construct multiple scattering contrast images (where portions of the transmitted beam are stopped by annular masks before they are detected) [10].

A second option is simply to average the measured energies. However, with small numbers of transmitted ions at each pixel, this method can produce some undesirable artifacts. Averages (or means) are sums over energy weighted probabilities and outlying

events can have a large effect on the average. To lessen the effect that outlying events have on the average, an energy window can be set and only ions whose energies fall within this window are energy averaged. However, care must be taken not to exclude ions containing valuable information.

A third method is to select the median value of transmitted energy, as suggested by Overley *et al.* [11]. They found median filtering discarded outlying values, efficiently eliminated 'speckle noise' (from sources such as slit scattering of ions) and tended to select the most likely residual ion energy at each beam location. They also noted that median filtering preserved edges and could faithfully reproduce monotonic functions such as ramps. However it could severely distort or suppress other features which produced only outlying values of energy loss. For instance a circular speck of increased or decreased thickness with diameter $< 2.36\sigma$ in an otherwise uniform field could be lost in a two dimensional scan area using a Gaussian of revolution and standard deviation σ for the incident beam profile [11]. Overley *et al.* suggested that energy averaging may be useful in these instances and also in measurements of beam profile diagnostics. They concluded that, for general image production, median filtering was the method of choice for small numbers of ions when compared to energy averaging or summing the number of ions within set energy limits. Similar conclusions have been reached at other microprobe facilities [8, 12].

As Lefevre *et al.* [4] noted, a distinction, can be made between images where the contrast parameter is number of selected ions to those where the contrast parameter is energy loss of individual ions. Counting statistics contribute to noise in an image when ions within an energy window are summed. On the other hand, if the contrast parameter is ion energy loss the statistics of straggling affect the image. Both median filtering and energy averaging can improve the accuracy of a energy loss measurement by utilising the information from nearly all the transmitted ions within a pixel. This improvement is important because, without it, the accuracy for each pixel is limited by energy straggling in the specimen, by energy resolution of the detector and by energy resolution of the accelerator. Lefevre *et al.* [7] have shown that, at least in theory, the effect of these can be arbitrarily reduced by taking the average/median of a sufficient number of ion

energy loss measurements. However, warning should be given that, although for a normal distribution of ion energy losses the average/median will converge to the most likely value, the average/median value may converge to unlikely values if the spectrum is complex.

In this review paper of STIM techniques we will limit our field of discussion to techniques that use energy loss contrast STIM.

STIM with energy loss contrast.

STIM, with energy loss contrast, is a quantitative, high resolution imaging technique. Due to the simple relationship between energy loss and projected density [4] the energy loss of each ion gives a measure of areal density within a few nm's of the ions path. The accuracy one can achieve in the areal density determination of a pixel with data from one or a few ions has been described elsewhere [5, 7]. Because ion-electron scattering angles are small owing to the ion-electron mass difference and because nuclear scattering events are rare when an ion beam slows down in a specimen, a MeV ion beam suffers a minimal spreading in quite thick samples . The loss in spatial resolution is usually only a few percent of the actual thickness of the specimen. This small scattering makes it possible to observe fine details within semi-thick specimens.

The technique is highly efficient as almost every ion carries useful information from which quantitative data can be obtained. The high efficiency of data collection, at present, necessitates the use of small beam currents (typically several thousand ions/second). Therefore small apertures must be used. Since both the first order spot size and the limiting resolution caused by lens aberrations fall at least as fast as aperture diameter, the beam spot size with STIM is smaller than that of other modalities which require higher beam currents. STIM is now and probably always will be the highest resolution imaging modality of MeV ion microprobes. Spatial resolutions as fine as 50 nm have been obtained [12]. The high efficiency of data collection also makes it possible to collect large data sets, even for high resolution STIM tomography with a small radiation dose.

Figure 1 shows a 2 MeV alpha particle energy loss contrast STIM image of a shadow

cast carbon replica of a diffraction line grating. The line spacing is 0.463 μm and the grating line width is $\sim$0.1 μm. The image size is 8.1 $\times$ 7.6 μm and consists of 132 $\times$ 124 pixels. At each pixel the mean value of at least 5 residual ion energies is displayed. Energy losses for these pixels vary between 11 and 50 keV. The image consists of 32 grey levels spanning a linear scale with darker regions representing higher energy losses. The spatial resolution displayed in the image is $\sim$100 nm. The mean energy loss at each pixel was subsequently converted to thickness using tabulated stopping powers for carbon at a density of 2.3 g/cm^3 [13]. The grating thickness varies between 35 nm and 155 nm and the image displays a thickness resolution of $\sim$20 nm. This figure shows the sensitivity of energy loss STIM to small changes in areal density. Even though the range in energy loss in the image is only 39 keV good energy loss contrast is obtained.

In order to identify boundaries and features of an area to be analysed via PIXE it is frequently necessary to have an image of better spatial resolution than that obtainable during the elemental microanalysis. Often samples contain few surface features of interest in secondary electron imaging and little internal contrast for optical imaging. In these instances the information obtained from energy loss STIM images can be invaluable for the interpretation of PIXE elemental maps. Further, the use of moment STIM images can also provide valuable detail on unresolved structure within the specimen [14]. Figure 2 shows trace element maps of Fe and Cu superimposed on a light greyscale energy loss STIM image of a freeze dried, frozen cryosection of ileum tissue from a mottled mouse. In the STIM image of dimensions 68 $\times$ 68 μm and spatial resolution 200 nm we see a central villus with neighbouring villi on either side. Structure is visible within the central villus. The trace element data was obtained with a spatial resolution of 3 μm using PIXE before the registered energy loss STIM data were recorded. In figure 2 the Fe and Cu are seen to be more heavily localised in the outer cytoplasmic regions of the epithelial cells.

There is another important application of energy loss STIM data. The STIM map may be used quantitatively to normalise PIXE maps against specimen areal density. In some instances normalising PIXE data to energy loss STIM data may be preferable than normalising it to backscattering spectroscopy data. Such instances can arise when

the backscattered ion spectrum is complex or when the sample is sufficiently thick that, although ions can penetrate through the sample, ions backscattered from the rear surface of the specimen are stopped by the specimen before detection. For the data presented in figure 2b, the energy loss STIM data and Cu x-ray yield from the outer cytoplasmic regions of the epithelial cells in the central villus yield a Cu concentration of 942 ± 120 μg/g, whereas the Cu concentration in the interior area of the villus is 573 ± 87 μg/g. The average Cu concentration over the whole villus tip area is 812 ± 98 μg/g which is consistent with other measurements of Cu concentration within whole ileum of similar mice [15]. Fe was also found to be more highly concentrated in the outer cytoplasmic regions of the epithelial cells.

The dose and dose rate are currently so low for energy loss STIM that images can be obtained of a sample either prior to or after elemental microanalysis without fear of significantly damaging the specimen any further. To ensure high resolution, reproducible quantitative microanalysis of materials, especially those which are fragile or susceptible to beam damage, it is necessary to know if a sample has suffered structural rearrangement or otherwise deteriorated during analysis. Energy loss STIM images recorded prior to and after elemental analysis can help quantify specimen shrinkage, mass loss and changes in morphological detail. Figure 3 shows a plot of final mass/initial mass plotted against dose (J/kg) for *Drosophila melanogastor* brains that were prepared by freeze substitution in acetone. The brains were each scanned with a 3 MeV proton beam for various doses with a current of 150 pA focussed to a spot of 5 μm diameter. 3 MeV proton energy loss contrast STIM images were recorded on each brain both before and after the 150 pA irradiation. Energy losses in these STIM images were subsequently converted to areal densities and the brain mass was calculated by summing these areal densities and multiplying the sum by the area of a single pixel in the respective STIM images. Additionally, the energy loss STIM images revealed that each brain had shrunk during the 150 pA irradiation. This specimen shrinkage appeared to be directly linked with the same beam specimen interactions that caused the sample mass loss [5].

Stereoscopic STIM imaging.

Good stereo imaging requires low noise and a spatial resolution much smaller than the specimen thickness. These requirements are met with energy loss STIM. In this case median filtering is preferable to energy averaging as it usually results in lower noise levels which makes the stereo pair easier to fuse. Figure 4 shows a dorsal view energy loss contrast STIM stereo pair of a portion of a fruit fly brain. The two views were separated by an angular rotation of 10^0. The stereo pair reveals much information about the location of structures within the brain. For instance the esophageal canal (the low density region in the centre of each image) is seen to pass through the centre of the brain. STIM stereo pairs provide a quick means for qualitatively mapping the 3-dimensional shape of objects and determining the relative position, orientation and shape of their internal and external structures. The dose required to form a stereo pair causes minimal damage to the specimen. Stereo pairs could prove useful in the future for preliminary feature identification in relatively large specimens which have undergone minimal preparation for analysis. This technique could also be performed with an external beam if necessary [6]. Using knowledge obtained from the stereo pair, further specimen preparation (such as sectioning in the case of biological materials) could then be undertaken to best prepare features of interest for more detailed STIM and or PIXE analysis if required.

STIM Tomography.

In recent years STIM with energy loss contrast has been combined with computed tomography techniques to produce three dimensional renditions of a sample [8]. STIM tomography (or ion microtomography) yields the spatial variation of the density itself within the sample. With this technique it is possible to resolve sub-micron scale variations in density within the sample [16]. The data set requirements, experimental and reconstruction techniques for STIM tomography have been described elsewhere [5, 8, 17, 18]. Figure 5 shows a 4 MeV sagittal view, proton energy loss contrast STIM image of the head capsule and thorax of a freeze dried *Drosophila melanogastor*. The image size is 1.5 x 1.5 mm and consists of 256 x 256 pixels. The incident beam was focussed to

a spot size of ~5 μm in diameter. Each pixel represents the median residual ion energy of 11 events and whiter areas indicate larger proton energy losses. This figure indicates that, although there is much structure within the head capsule and thorax, the spatial distribution of this structure cannot be adequately determined from a single STIM image without prior knowledge of the specimen.

Figure 6 shows a STIM tomography reconstruction of a plane through the thorax. The reconstructed plane corresponds to ~row 128 of the 256 rows of pixels in figure 5. The short black horizontal bars to the left and right of the image in figure 5 locate the approximate position of the plane. This tomogram was formed from 180 projections of the plane recorded at evenly spaced angles over an 180^0 rotation of the sample. At each sample point within a projection the median residual ion energy of 13 incident 4 MeV protons was determined. The median residual ion energies were converted to areal density assuming the chemical composition of the thorax was $C_5H_9O_2N$ [4]. The projection data were centre of mass pre-processed [5] and the plane was reconstructed using a filtered backprojection algorithm.

In figure 6, darker regions indicate higher densities. The image size is 1.5 × 1.5 mm and consists of 256 × 256 pixels. The large black arrow in the image denotes the direction of the incident beam used to record the energy loss STIM image in figure 4. The dorsal surface, (D), points towards the lower left corner of the image. The exoskeleton of the *Drosophila* is visible as is much structure within the thorax. On the right hand surface of the thorax, structure associated with the root of a wing, (R), is also visible. Most of the structure within the thorax is associated with the giant indirect flight muscles . The group of high density regions which are stacked one beneath the other in two columns are the dorsolongitudinal flight muscles, (DL). The majority of other high density regions on either side of the dorsolongitudinal muscles are the dorsoventral flight muscles, (DV). These muscles extend dorsoventrally in the lateral portions of the thorax. Towards the ventral surface, (V), of the thorax there are two high density regions, (F), of size ~100 × 100 μm. These regions most probably correspond to muscle groups associated with the forelegs. The reconstruction gives the density of these flight and leg muscles as varying between 1 and 1.5 g/cm^3. However, there are many other regions within the thorax

that have a density of <0.1 g/cm^3. Freeze drying has probably removed most of the fluid within the specimen. This loss of fluid probably contributes to the magnitude of the density variation within the specimen. Figure 6 exemplifies the advantage of STIM tomography for resolving features within an extended specimen.

The resolvable detail in a tomographic image is affected by the accuracy of the projected density determination for each sample point, the number of projections, the number of sample points per projection and the reconstruction algorithm. However, the primary variable in obtaining fine spatial resolution is the size of the beam spot profile. When energy losses are large, density variation determinations can be very accurate, but beam spatial broadening may be significant. To minimise spatial broadening heavy ions are usually preferable to light ions, assuming sufficiently high incident energies can be achieved [19]. Alternatively, for a given ion species, higher beam energies will minimise spatial broadening. For spatially thick specimens, spatial broadening resulting from the convergence angle of the focussed beam may also limit the spatial resolution at a given depth in the specimen. Recently, a reconstruction algorithm has been developed that approximately corrects for the effect of beam spatial broadening in specimens with suitable composition and geometry [5]. Future development of similar algorithms will promise finer spatial resolution studies of a broad range of specimens. Likewise, application of algorithms that can reconstruct a specimen from a limited set of projection measurements or reconstruct specimens with non-uniform chemical composition will also increase the range of specimens that can be analysed accurately.

The ability to efficiently acquire and analyse data can limit the size and nature of specimens that can be examined with high spatial resolution. Further, STIM tomography can require large amounts of computer memory for data storage. At present residual ion energies are usually measured with silicon surface barrier charged particle detectors and a peak detect style ADC which limits count rates to ~20,000 ions/second. Saint *et al.* [20] have calculated that, to create a complete three dimensional reconstruction of a 50 μm specimen with a 50 nm incident beam size, at least 1.5×10^{10} ions are required if the median value of residual ion energy at each sample point is formed from 10 ions. At a count rate of 20,000 ions/second it would take ~9 days to collect the required data.

From a practical viewpoint in order to achieve high resolution tomograms of large objects data acquisition rates need to be increased. Pontau *et al.* [21] have used time of flight energy loss measurements which could enable count rates of up to a few 10^5 ions/second. However, as data acquisition rates improve, data reduction and analysis rates will also have to be improved to take full advantage of this increase in efficiency.

STIM tomography is being developed as a powerful tool for characterising the density distribution within a variety of specimens. It may be preferable to x-ray microtomography in cases where low total density or small density variations make x-ray analysis difficult. Applications for STIM tomography have already developed in biology, chemistry, geology and materials science. Future improvements in data acquisition and analysis rates, reconstruction techniques and microprobe technology promise an increase in the range of specimens that can be examined at high spatial resolution with this technique. Because STIM tomography is non-invasive and because of its relatively low radiation dose, it may prove possible to study contained *in vivo* biological specimens which cannot be studied with conventional techniques. Future improvements in data acquisition rates may also make it possible to study dynamic systems. STIM tomography data may also find use in providing specimen densities and information about sample microstructure to mass normalise PIXE tomography data.

Channeling STIM.

In a thin single crystal, ion channeling can be used to modify the stopping power and provide contrast in an energy loss contrast STIM image. This technique is called Channeling STIM or CSTIM [9]. CSTIM is a very efficient technique and hence creates negligible crystal damage compared to larger ion beam doses and dose rates used in backscattering Channeling Contrast Microscopy (CCM). The very low beam current requirement enables very good channeling collimation and very good spatial resolution. Beam spread in the specimen due to the focusing cone angle does not occur for channeled particles. Even in semi-thick specimens this spatial resolution should not be substantially degraded until the point, if any, where dechanneling occurs. Due to the high efficiency,

CSTIM data require little time to collect and due to the low beam currents there is little problem with carbon build up on the specimen or increase in specimen temperature. CSTIM requires the use of thin specimens, but for such specimens if offers very high sensitivity for the detection of subsurface crystal disorder and imaging of sub-surface structures [9]. The high sensitivity of CSTIM to crystal damage allows us to utilise it to map damage profiles caused by higher ion beam doses and dose rates. Figure 7 shows median residual ion energy loss CSTIM greyscale maps of a 50 × 50 μm area of a 58 μm thick Si crystal. These CSTIM data were obtained with a sub-micron 3.9 MeV proton beam incident along the < 111 > axial direction of the crystal. After the upper image was recorded but, before the lower image was recorded, a stationary 3.9 MeV proton beam focussed to a spot of ~21 × 15 μm was used to irradiate the crystal until 5.8 μC of charge had been collected. The incident 1 nA beam for this irradiation was also incident along the < 111 > axial direction of the crystal. The CSTIM image recorded after the 5.8 μC dose clearly shows the damaged area. The increase in energy loss is due to crystal damage and dechanneling resulting from the 5.8 μC dose. Subsequent analysis revealed that energy loss differences of ~10 keV could be resolved in the image recorded after the 5.8 μC irradiation. CSTIM may provide a viable alternative for samples (such as poly-crystalline materials) that are prone to damage when analysed with backscattered CCM or analyses that require fine spatial resolution. It may also find a possible application in the investigation of crystal damage and small size imperfections in crystals <1 μm thick, especially if further development of STIM results in spot sizes which have dimensions of a few nm.

Conclusion.

STIM with energy loss contrast is a versatile technique that already has a wide range of applications. With future improvements in microbeam technology and computing power, combined with the fact that in the past two years several microprobe facilities have started to investigate the potential of STIM, an increased range of applications is to be expected.

Acknowledgements.

The authors wish to acknowledge the collaboration of H.W. Lefevre and R.M.S. Schofield from the University of Oregon, Eugene, U.S.A for the tomographic data of the fruit fly presented in this paper. This data was collected with the University of Oregon microprobe. The authors gratefully acknowledge the assistance of B.J. Kirby for preparing the mouse ileum tissue shown in figure 2. The authors also wish to acknowledge the support of a grant from the Australian research council. The writing of this paper was performed under the auspices of the U.S. Department of Energy by the Lawrence Livermore National Laboratory under contract number W-7405-Eng-48.

Figure Captions.

FIGURE 1 : 2 MeV alpha particle energy loss contrast STIM image of a shadow cast carbon replica of a diffraction line grating. The image size is 8.1 × 7.6 μm.

FIGURE 2 : Trace element maps (black dots) of (A) Fe and (B) Cu superimposed on a greyscale energy loss STIM image of mouse ileum tissue. Darker regions in the STIM image represent higher energy losses. The image size is 68 × 68 μm.

FIGURE 3 : Final mass / initial mass plotted against dose (J/kg) for the Drosophila brains irradiated with a 150 pA, 3 MeV scanned, focussed microbeam. The solid line is to guide the eye.

FIGURE 4: Dorsal view energy loss contrast STIM stereo pair of a portion of a *Drosophila melanogastor* brain. Each view has dimensions 290 × 480 μm. Each image was formed from the measured energy losses of 3 MeV protons.

FIGURE 5 : 4 MeV proton energy loss contrast STIM image of the head capsule and thorax of a *Drosophila melanogastor*. The image size is 1.5 × 1.5 mm and lighter areas indicate larger proton energy losses. The data were collected with the Eugene microprobe in collaboration with H.W. Lefevre and R.M.S. Schofield.

FIGURE 6 : Reconstruction of a slice through the thorax of a fruit fly. The image size is 1.5 × 1.5 mm and darker regions indicate higher densities. The labels on this figure are discussed in the text. The data for this image were collected with the Eugene microprobe in collaboration with H.W. Lefevre and R.M.S. Schofield.

FIGURE 7 : Median residual ion energy loss CSTIM greyscale maps of a 58 × 50 μm area of a 50 μm thick Si crystal before and after irradiation with a 1 nA 3.9 MeV proton beam focussed to a spot of ~15 × 21 μm. The image after this 5.8 μC dose clearly shows the damaged area of the specimen.

References.

1.) J.C. Overley, R.C. Connolly, G.E.Seiger, J.D. MacDonald and H.W. Lefevre, Nucl. Instr. and Meth 218 (1983) 43.

2.) R.M. Sealock, A.P. Mazzolini and G.J.F. Legge, Nucl. Instr. and Meth. 218 (1983) 217.

3.) B.E. Fischer,Nucl. Instr. and Meth. B10/11 (1985) 693.

4.) H.W. Lefevre, R.M.S. Schofield, J.C. Overley and J.D. MacDonald, Scanning Microscopy 1 (1987) 879.

5.) G. Bench, Ph.D. Thesis, University of Melbourne, unpublished, (1991).

6.) H.W. Lefevre, R.M.S. Schofield and D.R. Ciarlo, Nucl. Instr. and Meth. B54 (1991) 47.

7.) H.W. Lefevre, R.M.S. Schofield, G.Bench and G.J.F. Legge, Nucl. Instr. and Meth. B54 (1991) 383.

8.) A.E. Pontau, A.J. Antolak, D.H. Morse, A.A. Ver Berkmoes, J.M. Brase, D.W. Heikkinen, H.E. Martz and I.D. Proctor, Nucl. Instr. and Meth. B40/41 (1989) 646.

9.) M. Cholewa, G. Bench, G.J.F. Legge and A. Saint, Appl. Phys. Lett. 56 (1990) 1236.

10.) R.M. Sealock, D.N. Jamieson and G.J.F. Legge, Nucl. Instr. and Meth. B29 (1987) 557.

11.) J.C. Overley, R.M.S. Schofield, J.D. MacDonald, and H.W. Lefevre, Nucl. Instr. and Meth. B30 (1988) 337.

12.) G. Bench and G.J.F. Legge, Nucl. Instr. and Meth. B40/41 (1989) 655.

13.) H.H. Anderson and J.F. Ziegler, Helium Stopping Power and Ranges in All Elements (Permagon, New York, 1977).

14.) G. Bench, H.W. Lefevre and G.J.F. Legge, Nucl. Instr. and Meth. B54 (1991) 390.

15.) J. Camakaris, J.R. Mann and D.M. Danks, Nucl. Instr and Meth, Biochem. J. 180

(1979) 597.

16.) G. Bench, K.A. Nugent, M. Cholewa, A.Saint and G.J.F. Legge, Nucl. Instr. and Meth, B54 (1991) 390.

17.) A.E. Pontau, A.J. Antolak and D.H. Morse, Nucl. Instr. and Meth. B54 (1991) 383.

18.)A.E. Pontau, A.J. Antolak and D.H. Morse, Nucl. Instr. and Meth. B45 (1990) 503.

19.) B.E. Fischer and C. Muhlbauer, Nucl. Instr. and Meth., B47 (1990) 271.

20.) A. Saint, G. Bench, M. Cholewa, S. Dooley, D.N. Jamieson and G.J.F Legge, Nucl. Instr and Meth. B56/57 (1991) 717.

21.) A.E. Pontau, D.H. Morse and M.R. Roberts, Private Communication (1992).

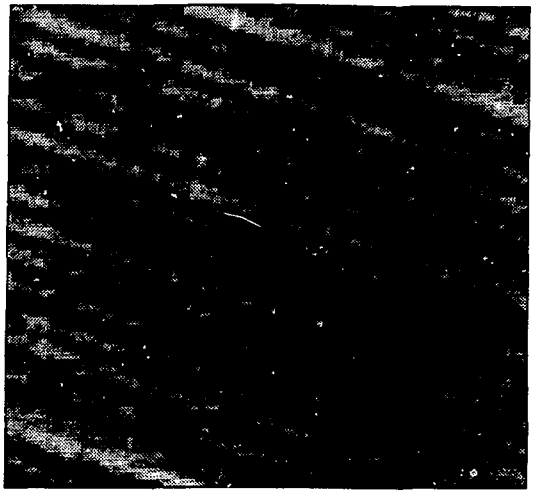

Figure1

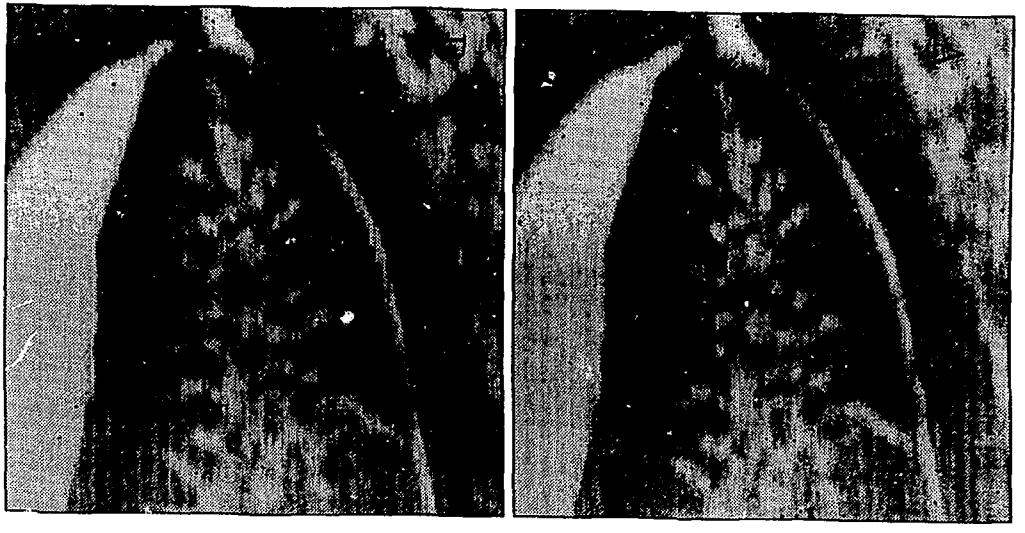

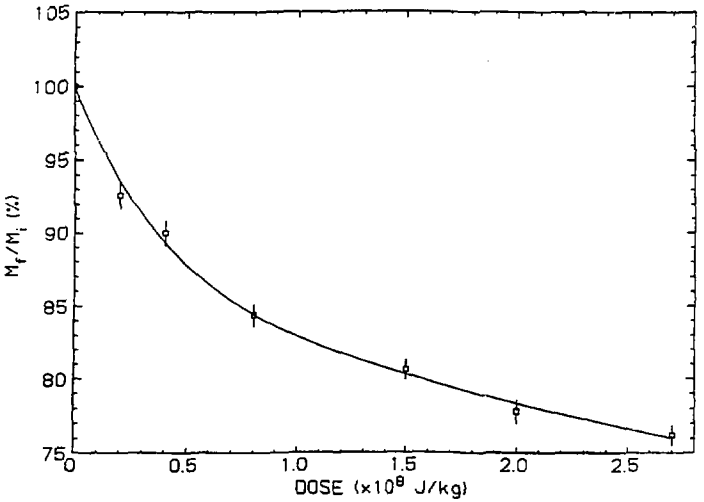
105
100
95
90
85
80
75
0
0.5
1.0
1.5
2.0
2.5
M_f/M_i (%)
DOSE ($\times 10^8$ J/kg)

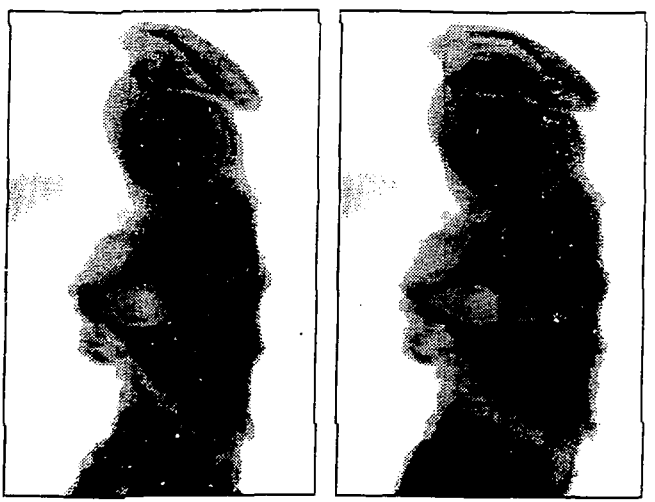

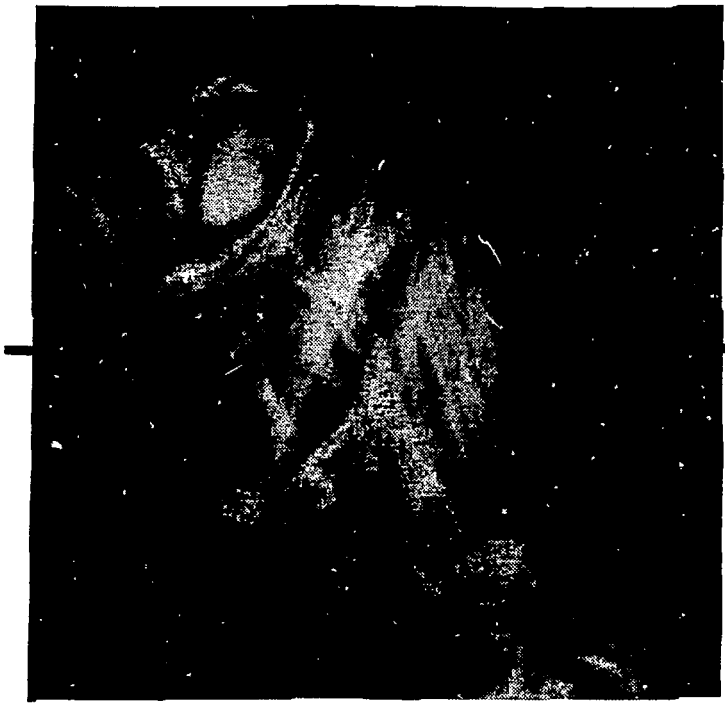


V
F
PV
SL
PV
R
D

BEFORE

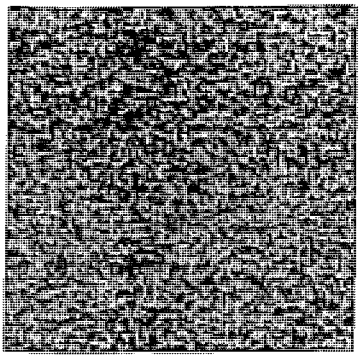

AFTER